J|A|C|S
ARTICLES
Published on Web 11/21/2002

Oxidation of Heme to β- and δ-Biliverdin by *Pseudomonas aeruginosa* Heme Oxygenase as a Consequence of an Unusual Seating of the Heme

Gregori A. Caignan,[†] Rahul Deshmukh,[‡] Angela Wilks,*[,‡] Yuhong Zeng,[†] Hong-wei Huang,[§] Pierre Moënne-Loccoz,[§] Richard A. Bunce,[†] Margaret A. Eastman,[†] and Mario Rivera*[,†]

Contribution from the Department of Chemistry, Oklahoma State University, Stillwater, Oklahoma 74078, Department of Pharmaceutical Sciences, School of Pharmacy, University of Maryland, Baltimore, Maryland 21201-1180, and Department of Biochemistry and Molecular Biology, OGI School of Science and Engineering at OHSU, Beaverton, Oregon 97006-8921

Received June 27, 2002

Abstract: The origin of the unusual regioselectivity of heme oxygenation, i.e. the oxidation of heme to δ-biliverdin (70%) and β-biliverdin (30%), that is exhibited by heme oxygenase from *Pseudomonas aeruginosa* (*pa*-HO) has been studied by ^{1}H NMR, ^{13}C NMR, and resonance Raman spectroscopies. Whereas resonance Raman indicates that the heme−iron ligation in *pa*-HO is homologous to that observed in previously studied α-hydroxylating heme oxygenases, the NMR spectroscopic studies suggest that the heme in this enzyme is seated in a manner that is distinct from that observed for all other α-hydroxylating heme oxygenase enzymes for which a structure is known. In *pa*-HO, the heme is rotated in-plane ∼110°, so the δ-meso-carbon of the major orientational isomer is located within the HO-fold in the place where the α-hydroxylating enzymes typically place the α-meso-carbon. The unusual heme seating displayed by *pa*-HO places the heme propionates so that these groups point in the direction of the solvent-exposed heme edge and appears to originate in large part from the absence of stabilizing interactions between the polypeptide and the heme propionates, which are typically found in α-hydroxylating heme oxygenase enzymes. These interactions typically involve Lys-16 and Tyr-112, in *Neisseriae meningitidis* HO, and Lys-16 and Tyr-134, in human and rat HO-1. The corresponding residues in *pa*-HO are Asn-19 and Phe-117, respectively. In agreement with this hypothesis, we found that the Asn-19 Lys/Phe-117 Tyr double mutant of *pa-HO* exists as a mixture of molecules exhibiting two distinct heme seatings; one seating is identical to that exhibited by wild-type *pa*-HO, whereas the alternative seating is very similar to that typical of α-hydroxylating heme oxygenase enzymes and is related to the wild-type seating by ∼110° in-plane rotation of the heme. Furthermore, each of these heme seatings in the *pa*-HO double mutant gives rise to a subset of two heme isomeric orientations that are related to each other by 180° rotation about the α−γ-meso-axis. The coexistence of these molecules in solution, in the proportions suggested by the corresponding area under the peaks in the ^{1}H NMR spectrum, explains the unusual regioselectivity of heme oxygenation observed with the double mutant, which we found produces α- (55%), δ- (35%), and β-biliverdin (10%). α-Biliverdin is obtained by oxidation of the heme seated similar to that of α-hydroxylating enzymes, whereas β- and δ-biliverdin are formed from the oxidation of heme seated as in wild-type *pa*-HO.

Introduction

Heme oxygenase (HO) oxidatively cleaves heme to biliverdin with the release of iron and CO.[1,2] The heme oxygenase reaction consumes three molecules of oxygen and a total of seven electron equivalents in the form of NADPH to convert one heme molecule to biliverdin.[2−4] The transfer of electrons from NADPH to the mammalian enzyme is mediated by cytochrome P450 reductase.[5] The bacterial HOs, like their mammalian counterparts, are NADPH-dependent enzymes that catalyze the oxidation of heme to biliverdin by a mechanism similar to that described for the mammalian enzymes.[6−8] Whereas HO in mammals functions to maintain heme homeostasis, the role of

* To whom correspondence should be addressed. M.R. e-mail: rivera@okstate.edu. A.W. e-mail: awilks@rx.umaryland.edu.
[†] Department of Chemistry, Oklahoma State University.
[‡] University of Maryland.
[§] OGI School of Science and Engineering at OHSU.

(1) Tenhunen, R.; Marver, H., S.; Schmid, R. *J. Biol. Chem.* **1969**, *244*, 6388−6394.
(2) Ortiz de Montellano, P. R.; Wilks, A. *Adv. Inorg. Chem.* **2000**, *51*, 359−407.
(3) Liu, Y.; Lightning, L. K.; Huang, H.; Moënne-Loccoz, P.; Schuller, D. J.; Poulos, T. L.; Loehr, T. M.; Ortiz de Montellano, P. R. *J. Biol. Chem.* **2000**, *275*, 34501−34507.
(4) Ortiz de Montellano, P. R. *Curr. Opin. Chem. Biol.* **2000**, *4*, 221−227.
(5) Yoshida, T.; Noguchi, M.; Kikuchi, G. *J. Biol. Chem.* **1980**, *255*, 4418−4420.
(6) Wilks, A.; Schmitt, M. P. *J. Biol. Chem.* **1998**, *273*, 837−841.
(7) Chu, G. C.; Tomita, T.; Sönnichsen, F. D.; Yoshida, T.; Ikeda-Saito, M. *J. Biol. Chem.* **1999**, *274*, 24490−24496.

bacterial heme oxygenases appears to revolve around the breakdown of heme with the purpose of providing the bacterium with the ability to use heme as a source of iron.[9−11] Although the nature of several of the intermediates in the heme oxygenation reaction has been determined, the relationship between protein structure and factors such as ligand discrimination, oxygen activation, and regiospecificity are not yet well understood. The recent crystal structures of *Neisseriae meningitidis* HO[12] (*nm*-HO) and h-HO-1[13] demonstrated that, unlike the globins or the peroxidases, HOs do not have a distal histidine or a distal polar residue that may help stabilize an O_2 or −OOH ligand. However, the crystal structures suggest that the carbonyl and NH groups of conserved glycine residues (139 and 143 in h-HO-1) may carry out this role. Moreover, the flexibility imparted by these residues to the distal helix appears to be important for heme oxygenase catalytic activity. In agreement with this hypothesis, replacement of Gly-139 or Gly-143 with bulkier amino acids suppresses heme oxygenase activity, and in some cases, the mutants acquire peroxidase activity.[3,14]

Insights gained from the crystal structures of the bacterial[12] and mammalian HOs[13,15] suggest that the regioselectivity of the reaction is likely to be controlled by steric interactions between the distal helix and the heme, which restrict attack of the Fe^{III}−OOH oxidizing species to the β-, γ-, and δ-meso-carbons. Electronic factors have also been implicated in the control of regiospecificity on the basis that electron-donating and electron-withdrawing substituents located on a meso-carbon exert a different influence on the regioselectivity of heme cleavage performed by HO.[16,17] More recently, magnetic resonance studies conducted with models of the low-spin Fe^{III}−OOH intermediate of HO suggest that this key intermediate exists as an equilibrium mixture consisting of a planar heme with a $(d_{xy})^2(d_{xz},d_{yz})^3$ electron configuration and a ruffled heme with a $(d_{xz},d_{yz})^4(d_{xy})^1$ electron configuration.[18] At ambient temperatures the equilibrium favors the $(d_{xy})^1$ electron configuration, and the ruffled porphyrinate ring is expected to aid the attack of the terminal oxygen of the Fe^{III}−OOH intermediate on the meso-carbon. In addition, the large spin density at the meso-carbons of a low-spin ferric heme possessing a $(d_{xy})^1$ electron configuration suggests the possibility of a radical mechanism for HO.[18] It is therefore conceivable that the regioselectivity of oxidative heme degradation is controlled by a combination of steric and electronic factors, where the ruffled $(d_{xy})^1$ heme places a pair of meso-carbons (α and γ, or β and δ) closer to the terminal OH of Fe^{III}−OOH at any given moment. Steric interactions between the distal pocket and the heme are likely to determine which pair of meso-carbons is positioned closer to the coordinated peroxide, and steric interactions are also likely to determine which meso-carbon from a pair (e.g. α or γ) is attacked.[18]

Recent characterization of heme oxygenases from *Corynebacterium diphtheriae* (*cd*-HO)[6] and *Neisseriae meningitidis* (*nm*-HO)[7] revealed that these enzymes hydroxylate heme exclusively at the α-meso-position, like the previously characterized mammalian proteins. In contrast, the *Pseudomonas aeruginosa* heme oxygenase (*pa*-HO),[8] which is 37% identical in amino acid sequence to *nm*-HO, hydroxylates heme predominantly at the δ-meso-position. The study of *pa*-HO, therefore, is likely to provide additional insights into the factors that control the regioselectivity of oxidative cleavage during the process of heme catabolism.

As an initial step toward this goal, amino acid sequence alignments carried out in the context of the available X-ray crystal structures revealed that Lys-16 and Tyr-112 in *nm*-HO (Lys-16 and Tyr-134 in h-HO-1 and r-HO-1), which form hydrogen-bonding and ionic interactions with the heme propionates, have been replaced by Asn-19 and Phe-117 in *pa*-HO. These observations led us to hypothesize that if the fold in *pa*-HO is similar to that of the other bacterial and mammalian HOs, δ-hydroxylation may be a consequence of the alternative interactions experienced by the heme propionates that result in a heme seating different from that observed in the mammalian and *nm*-HOs. As will be shown below, NMR spectroscopic evidence strongly suggests that the heme seating in *pa*-HO is rotated ∼110° from the heme seating common to the other known bacterial and mammalian heme oxygenases. It will also be shown that upon replacing Asn-19 and Phe-117 for Lys and Tyr, respectively, the heme in the double mutant enzyme experiences a dynamic equilibrium between two heme seatings, one identical to that of wild-type *pa*-HO, and the other typical of the previously characterized α-selective heme oxygenases. In addition, the double mutant exhibits altered regioselectivity in which both α- and δ-biliverdin products are observed, reflecting the dynamic equilibrium of the two heme seatings in the double mutant.

Experimental Section

General Methods. Plasmid purification, subcloning, and bacterial transformations were carried out as previously described.[19] Deionized, doubly distilled water was used for all experiments. Oligonucleotides were obtained from Sigma-Genosys and used without further purification. All absorption spectra of the heme−HO complexes were recorded on a Cary Varian 1E UV spectrophotometer.

Bacterial Strains. *Escherichia coli* strain DH 5α [F′, *ara* D(*lac-proAB*) rpsL ø80d*lacZ*DM15 *hsd* R17] was used for DNA manipulation and *E. coli* strain BL21 (DE3) pLysS [F^- *ompT hsdS*$_B$ ($r_B^-m_B^-$) *gal dcm* (DE3)] was used for expression of both the wild-type and mutant heme oxygenase constructs.

Mutagenesis of pEHmuO. Mutagenesis was carried out by polymerase chain reaction using the Quickchange Mutagenesis Kit from Stratagene (La Jolla, CA). Oligonucleotides were designed to have melting temperatures (T_m) between 65 and 75 °C. All mutations were verified by DNA sequencing, which was carried out at the Biopolymer Laboratory, School of Medicine, University of Maryland, Baltimore.

(8) Ratliff, M.; Zhu, W.; Deshmukh, R.; Wilks, A.; Stojilkovic, I. *J. Bacteriol.* **2001**, *183*, 6394−6403.
(9) Stojiljkovic, I.; Hantke, K. *EMBO J.* **1992**, *11*, 4359−4367.
(10) Stojiljkovic, I.; Hantke, K. *Mol. Microbiol.* **1994**, *13*, 719−732.
(11) Zhu, W.; Hunt, D. J.; Richardson, A. R.; Stojiljkovic, I. *J. Bacteriol.* **2000**, *182*, 439−447.
(12) Schuller, D. J.; Zhu, W.; Stojiljkovic, I.; Wilks, A.; Poulos, T. L. *Biochemistry* **2001**, *40*, 11552−11558.
(13) Schuller, D. J.; Wilks, A.; Ortiz de Montellano, P. R.; Poulos, T. L. *Nature Struct. Biol.* **1999**, *6*, 860−867.
(14) Koenigs Lightning, L.; Huang, H.; Moënne-Loccoz, P.; Loehr, T. M.; Schuller, D. J.; Poulos, T. L.; Ortiz de Montellano, P. R. *J. Biol. Chem.* **2001**, *276*, 10612−10619.
(15) Sugishima, M.; Omata, Y.; Kakuta, Y.; Sakamoto, H.; Noguchi, M.; Fukuyama, K. *FEBS Lett.* **2000**, *471*, 61−66.
(16) Torpey, J.; Lee, D. A.; Smith, K. M.; Ortiz de Montellano, P. R. *J. Am. Chem. Soc.* **1996**, *118*, 9172−9173.
(17) Torpey, J.; Ortiz de Montellano, P. R. *J. Biol. Chem.* **1997**, *272*, 22008−22014.
(18) Rivera, M.; Caignan, G. A.; Astashkin, A. V.; Raitsimring, A. M.; Shokhireva, T. K.; Walker, F. A. *J. Am. Chem. Soc.* **2002**, *124*, 6077−6089.
(19) Sambrook, J.; Fritsch, E. F.; Maniatis, T. *Molecular Cloning*: *A Laboratory Manual*, 2nd ed.; Cold Spring Harbor Press: Cold Spring Harbor, NY, 1989.

Expression and Purification of Wild-Type and Mutant *pa*-HOs. The wild-type heme oxygenase proteins and their corresponding mutants were purified as previously described.[8] A single colony of freshly transformed *E. coli* BL21 (DE3) plysS cells was cultured overnight in 5 mL of LB-medium containing 100 μg/mL of ampicillin. The cells were subsequently subcultured into fresh LB−ampicillin medium (100 mL) and grown at 37 °C to mid-log phase. The cells were then subcultured (10 mL) into LB−ampicillin media (1 L) and on reaching mid-log phase expression was induced by addition of isopropyl-1-thiol-D-galactopyranoside (IPTG) to a final concentration of 1 mM. The cells were grown further for 4−5 h at 30 °C and harvested by centrifugation (10000*g* for 20 min). Cells were lysed by sonication in 50 mM Tris-HCl (pH 7.8) containing 1 mM EDTA and 1 mM phenylmethysulfonyl fluoride (PMSF). The cell suspension was then centrifuged at 27000*g* for 40 min. The soluble fraction was applied to a Sepharose-Q Fast Flow column (1.5 × 10 cm) previously equilibrated with 20 mM Tris-HCl (pH 7.5). The column was washed with 3 volumes of 20 mM Tris-HCl (pH 7.5) containing 50 mM NaCl. The protein was then eluted with the same buffer with a linear gradient of NaCl from 50 to 500 mM. The protein eluted at a concentration of 150 mM NaCl, and the peak fractions were pooled and dialyzed against 10 mM potassium phosphate (pH 7.4) (2 × 4 L) at 4 °C. The *pa*-HO protein was then stored at −80 °C or reconstituted with heme as described below.

Reconstitution of the Wild-Type and *pa*-HO Mutants. The heme−HO complexes were prepared as described previously.[20] Hemin was added to the purified HO proteins at a final 2:1 heme:protein ratio. The sample was then applied to a Q-sepharose column (1.5 × 6.0 cm) preequilibrated with 20 mM Tris-HCl (pH 7.8). The column was washed with equilibration buffer (5 volumes), followed by the same buffer containing 50 mM NaCl. The protein was then eluted with 20 mM Tris (pH 7.8) containing 250 mM NaCl. The protein fractions were pooled and dialyzed (2 × 4 L) against 20 mM Tris-HCl (pH 7.8) at 4 °C. The protein was concentrated by an Amicon filtration unit and stored at −80 °C. Samples for NMR and resonance Raman analysis were passed down a Sephacryl S-100 HR column (3.0 × 100 cm) following concentration on an Amicon Filtration unit.

Electronic Absorption Spectroscopy of the Wild-Type and Mutant *pa*-HOs. The UV−visible spectra of the wild-type HOs and their respective mutants were recorded in 20 mM Tris (pH 7.5). The Fe(II)−CO spectra were obtained by saturating the solution with CO followed by the addition of a few grains of sodium dithionite. The Fe(II)−O_2 complexes were obtained by passage of the Fe(II)−CO complexes through a Sephadex G-25 column (1.0 × 3.0 cm).

Determination of the Extinction Coefficient for the Heme−*pa*-HO Complexes. The millimolar extinction coefficient (ϵ_{405}) for the heme−HO complexes was determined as previously described.[21] The absorbance of a purified heme−HO sample at 405 nm was measured. An excess of dithionite was added and the spectrum of the reduced ferrous pyridine hemochrome was then recorded. The concentration was calculated from the absorbance maxima at 418.5, 526, and 555 nm using extinction coefficient values of 170, 17.5, and 34.4 mM, respectively.

Reaction of the Heme−*pa*-HO Complexes with NADPH Cytochrome P450 Reductase or Ascorbate. The reaction of the heme−HO complexes in the presence of NADPH reductase was carried out as previously described.[6] Purified human cytochrome P450 reductase was added to the heme−HO complex (10 mM) at a molar ratio of reductase:HO equal to 3:1 in a final volume of 1 mL of 20 mM Tris-HCl (pH 7.5). The reaction was initiated by the addition of NADPH in 10 mM increments to a final concentration of 100 mM. The spectral changes between 300 and 750 nm were monitored over a 30 min time period at 1 min intervals. Following completion of the reaction, the product was extracted for HPLC analysis as described below. The ascorbic acid dependent conversion of heme to biliverdin was also monitored. Ascorbic acid at a final concentration of 5 mM was added directly to the heme−HO complex (10 mM) in 20 mM Tris-HCl buffer (pH 7.5). The spectral changes between 300 and 750 nm were recorded over a 20 min time period. The products of the reaction were extracted and subjected to HPLC analysis as described below.

HPLC Analysis of Heme−*pa*-HO Reaction Products. Following the reaction of the heme−HO complexes with NADPH cytochrome P450 reductase or with ascorbate, glacial acetic acid (20 mL) and 3 M HCl (20 mL) were added to the reaction (1 mL) before extracting into chloroform. The organic layer was washed with distilled water (3 × 1 mL) and the chloroform layer removed under a stream of argon. The resultant residue was dissolved in 1 mL 4% sulfuric acid in methanol and esterified for 12 h at room temperature. The esters were diluted (4-fold) with distilled water and extracted into chloroform. The organic layer was washed further with distilled water, dried over sodium sulfate, and the chloroform was again removed under a stream of argon. The residue was dissolved in 85:15 (v/v) methanol:water prior to HPLC analysis. The samples were analyzed by reverse-phase HPLC on a ODS-AQ C18 (S-5) (YMC, Inc., Wilmington, NC) column (3.0 × 250 mm) eluted with 85:15 (v/v) methanol:water at a flow rate of 0.4 mL/min. The elutant was monitored at 380 nm and the biliverdin standards eluted in the order α (11.9 min), β (13.9 min), δ (14.8 min), and γ (18.5 min).[22] The ratio of isomers was calculated by integration of the peaks within each experiment and averaged for five separate experiments.

Preparation of HOs Reconstituted with ^{13}C-Labeled Heme. ^{13}C-Labeled δ-aminolevulinic acids (ALA) were used as biosynthetic precursors for the preparation of protoheme IX (heme). [3-^{13}C]-δ-aminolevulinic acid ([3-^{13}C-]ALA), [5-^{13}C]ALA, and [1,2-^{13}C]ALA were synthesized utilizing methods described previously.[23] Heme labeled with ^{13}C was obtained utilizing previously reported methodology,[24] which was developed to take advantage of the fact that the first committed precursor in heme biosynthesis is δ-aminolevulinic acid (ALA).[25,26] Thus, ^{13}C-labeled heme, which is biosynthesized in *E. coli* upon addition of suitably labeled ALA, is trapped by simultaneously expressing rat liver outer mitochondrial membrane cytochrome b_5 (OM cyt b_5).[24] The details of the biosynthetic protocol, which entail the expression and purification of OM cyt b_5 harboring ^{13}C-labeled heme, have been presented previously.[27] Reconstitution of HO with ^{13}C-labeled heme entails the removal of the isotopically labeled macrocycle from OM cyt b_5, followed by the formation of the heme−HO complex. A typical protocol used to extract ^{13}C-labeled heme from OM cyt b_5 follows: Pyridine (15 mL) is added to 2.5 mL of 1 mM OM cyt b_5 in phosphate buffer (μ = 0.10, pH = 7.0), while the temperature is maintained at 4 °C. Slow addition of chloroform, typically 10−15 mL, results in the precipitation of the polypeptide, while the pyridine hemochrome is maintained in the supernatant. The latter is subsequently separated from the denatured polypeptide by centrifugation, allowed to equilibrate at room temperature, and then dried over anhydrous $MgSO_4$. The desiccant is removed by filtration and the filtered pyridine−chloroform solution transferred to a round-bottom flask, where it is concentrated to dryness on a rotary evaporator. Finally, the resultant solid is redissolved in 3−4 mL of 0.1 M NaOH in the presence of a 10-fold excess of NaCN, and the pH adjusted to 9.5 (adjusting the pH to 9.5 in the absence of CN^- often results in heme aggregation and precipitation). HO is reconstituted with a freshly prepared solution of ^{13}C-labeled heme by titrating it into a 20 mL solution of 20 mM Tris containing ~2 μmol of HO until the ratio A_{280}/A_{Soret} no longer changes.

(20) Wilks, A.; Ortiz de Montellano, P. R. *J. Biol. Chem.* **1993**, *268*, 22357−22362.
(21) Fuhrop, J. H.; Smith, K. M. In *Porphyrins and Metalloporphyrins*; Smith, K. M., Ed.; Elsevier: Amsterdam, 1975; pp 804−807.
(22) Sakamoto, H.; Omata, Y.; Adachi, Y.; Palmer, G.; Noguchi, M. *J. Inorg. Biochem.* **2000**, *82*, 113−121.
(23) Bunce, R. A.; Shilling, C. L., III; Rivera, M. *J. Labeled Compd. Radiopharm.* **1997**, *39*, 669−675.
(24) Rivera, M.; Walker, F. A. *Anal. Biochem.* **1995**, *230*, 295−302.
(25) Warren, M. J.; Scott, A. I. *Trends Biochem. Sci.* **1990**, *15*, 426−431.
(26) Scott, A. I. *Angew. Chem.* **1993**, *32*, 1223−1376.
(27) Rivera, M.; Qiu, F.; Bunce, R. A.; Stark, R. E. *JBIC* **1999**, *4*, 87−98.

The resultant solution containing the cyanide-inhibited enzyme is then incubated at 4 °C overnight, dialyzed against 2.0 L of 10 mM phosphate (pH 7.5) over a period of 24 h, and then purified by chromatography. HO from *C. diphtheriae* was loaded onto a hydroxyapatite column (2 cm × 12 cm) equilibrated at 4 °C with 10 mM phosphate buffer, pH 7.5, and eluted with a linear phosphate gradient (10−150 mM). Those fractions containing pure protein were concentrated in Amicon centrifugal concentrators to approximately 1 mL and then transferred to smaller Centricon concentrators in order to exchange the protein into deuterated phosphate buffer, pH 7.5, not corrected for the deuterium effect. Purification of freshly reconstituted *pa*-HO was accomplished by loading it onto a Q-sepharose column (3 × 5 cm) and eluting it with a linear salt gradient (10−500 mM).

Resonance Raman Spectroscopy. Resonance Raman spectra were obtained on a McPherson 2061/207 spectrograph (0.67 m with variable gratings) equipped with a Princeton Instrument liquid N_2-cooled (LN-1100PB) CCD detector. Kaiser Optical supernotch filters were used to attenuate Rayleigh scattering. Excitation sources consisted of an Innova 302 krypton laser (413 nm), and a Liconix 4240NB He/Cd laser (442 nm). Spectra were recorded in a 90° scattering geometry on samples at room temperature. Frequencies were calibrated relative to indene and CCl_4 standards and are accurate to ±1 cm^{-1}. CCl_4 was also used to check the polarization conditions. Electronic absorption spectra of the samples used for Raman spectroscopy were obtained on a Cary 50 Varian spectrophotometer, to monitor the samples both before and after laser illumination.

NMR Spectroscopy. ^1H and ^{13}C spectra were acquired on a Varian Unity Inova spectrometer operating at frequencies of 598.611 and 150.532 MHz, respectively. ^1H spectra were referenced to the residual water peak at 4.8 ppm, and ^{13}C spectra were referenced to an external solution of dioxane (60% v/v in D_2O) at 66.66 ppm. Proton spectra were acquired with presaturation of the residual water peak over 15K data points, a spectral width of 30 kHz, a 250 ms acquisition time, a 200 ms relaxation delay, and 1024 scans. ^{13}C spectra were collected over 24K data points, a spectral width of 59 kHz, a 200 ms acquisition time, a 25 ms relaxation delay, and 400 000 scans. HMQC spectra[28] were typically acquired with spectral widths of 30 kHz for ^1H and 50 kHz for ^{13}C, respectively, and a 200 ms relaxation delay. HMQC spectra obtained from samples containing HO reconstituted with heme labeled using [1,2-^{13}C]ALA as a heme precursor (see Figure 3) were acquired with refocusing delays based on $^1J_{CH} = 140$ Hz, while data obtained from HO reconstituted with heme labeled using [5-^{13}C]ALA as the heme precursor were acquired with $^1J_{CH} = 180$ Hz. Data were collected as an array of 2K × 128 points with 512 scans per t_1 increment and processed by zero-filling once in t_2 and twice in t_1 to obtain an 8K × 8K matrix. This was apodized with a 90°-shifted squared sine bell function and Fourier transformed. WEFT NOESY[29,30] spectra were acquired with 29 kHz in both dimensions, 2K data points in t_2, 256 increments in t_1, 512 scans per t_1 increment, and (typically) a 40 ms mixing time. The data were processed by zero-filling in both dimensions to obtain an 8K × 8K matrix, apodized with 90°-shifted squared sine bell, and Fourier transformed. EXSY[31] data were acquired in a similar manner, except that the mixing time was set to 5 ms.

Results

Expression, Purification, and Spectral Characterization of the Wild-Type and Mutant *pa*-HOs. The wild-type and mutant *pa*-HOs were expressed and purified as previously described.[8] Each of the proteins was estimated to be >95% pure by SDS−PAGE (data not shown). The Soret maxima of the ferric (Fe^{III}) state of the wild-type and mutant proteins were essentially identical (Table 1). Upon reduction to the ferrous (Fe^{II}) state, the Fe^{II}−CO and Fe^{II}−O_2 complexes were in the range 420−421 and 410−413 nm, respectively (Table 1). Characteristic visible bands for the Fe^{III} charge-transfer bands and the Fe^{II}−CO or Fe^{II}−O_2 α/β bands in all the mutant proteins remained relatively unchanged from those of the wild-type protein (Table 1). These data suggest that the heme coordination in the mutant proteins was similar to that of the wild-type protein and were not grossly altered by the amino acid substitutions.

Table 1. Characteristic Features of the UV−Visible Spectra of Wild Type and Mutant Heme-*pa*-HO Complexes

	Soret maxima (nm)			visible bands (nm)			Soret extinction coefficient
enzyme	Fe^{III}	Fe^{II}–O_2	Fe^{II}−CO	Fe^{III}	Fe^{II}−O_2	Fe^{II}−CO	(mM^{-1} cm^{-1})
wild-type	406	410	421	630	577/541	570/540	130
Asn-19 Lys	407	413	420	630	577/541	570/538	127
Phe-117 Tyr	406	412	420	629	577/541	570/537	112
Asn-19 Lys/ Phe-117 Tyr	406	412	420	631	577/541	570/539	138

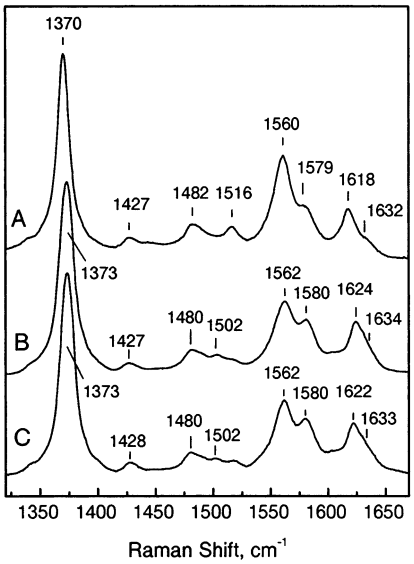

Figure 1. High-frequency region of the RR spectra of ferric heme−protein complexes in wild-type (wt) *nm*-HO (A), wt *pa*-HO (B), and N19K/F117Y *pa*-HO (C).

Resonance Raman Characterization. The high-frequency region of RR spectra of hemoproteins obtained with Soret excitation is dominated by porphyrin skeletal modes, which are indicative of the oxidation state, spin state, and coordination state of the heme iron.[32] In the ferric heme−*nm*-HO complex the ν_3 and ν_2 modes at 1482 and 1560 cm^{-1}, respectively, are characteristic of a six-coordinated, high-spin (6cHS) configuration. A minor six-coordinated, low-spin (6cLS) population is also evidenced by a red-shifted ν_{10} at 1632 cm^{-1} (Figure 1A). The ferric heme complexes of the wild-type and the Asn-19 Lys/Phe-117 Tyr double mutant of *pa*-HO exhibit nearly identical RR spectra, consistent with a mixture of 6cHS and 6cLS species (Figure 1B,C). The combined ν_4 modes of the 6cHS and 6cLS species are observed at 1373 cm^{-1} in *pa*-HO rather than at 1370 cm^{-1} in *nm*-HO, and distinct 6cLS ν_3 and ν_2 in *pa*-HO spectra at 1502 and 1580 cm^{-1}, respectively, are

(28) Summers, M. F.; Luigi, G. M.; Bax, A. *J. Am. Chem. Soc.* **1986**, *108*, 4285−4294.
(29) Patt, S. L.; Sykes, B. D. *J. Chem. Phys.* **1972**, *56*, 3182−3184.
(30) Lankhorst, P. P.; Wille, G.; van Boom, J. H.; Altona, C.; Haasnoot, C. A. G. *Nucl. Acids Res.* **1983**, *11*, 2839−2856.
(31) Jeneer, J.; Meier, B. H.; Bachmann, P.; Ernst, R. R. *J. Chem. Phys.* **1979**, *71*, 4546−4553.
(32) Spiro, T. G., Spiro, T. G., Ed.; John Wiley & Sons: New York, 1988; Vol. 3, pp 1−37.

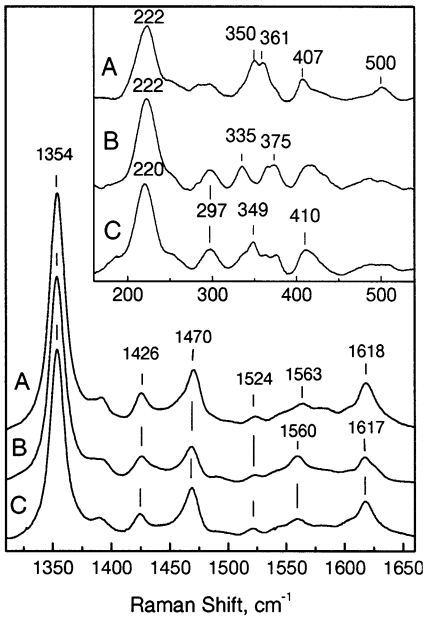

Figure 2. High-frequency region of the RR spectra of ferrous heme−protein complexes in *nm*-HO (A), wt *pa*-HO (B), and N19K/F117Y *pa*-HO (C). The inset shows the low-frequency region obtained with 442-nm excitation.

readily attributed to a greater content of 6cLS species in *pa*-HO than in *nm*-HO. Such mixtures of 6cHS/6cLS configurations are observed in the ferric HO-1 and *cd*-HO proteins and are attributed to the ligation of an ionizable water ligand in the distal pocket, trans to the proximal histidine ligand.[33,34]

Upon reduction to the ferrous state, all three heme protein complexes display RR spectra characteristic of pentacoordinated high-spin (5cHS) species (Figure 2). The dissociation of the sixth ligand present in the ferric heme upon reduction to the ferrous state further identifies this labile ligand as a water molecule. Most importantly, using 442-nm laser excitation, known to favor the resonance enhancement of iron−histidine stretching vibration in ferrous HS species, both *nm*-HO and *pa*-HO complexes show a strong RR band at 222 cm^{-1} (inset Figure 2). This vibration is also observed with similar bandwidth and intensity in the double mutant of *pa*-HO, although its frequency is shifted by −2 cm^{-1} to 220 cm^{-1}. The ν(Fe−His) mode is influenced by the microenvironment of the N_δ-His and ranges from ∼200 cm^{-1} in the absence of hydrogen-bonding interactions to ∼250 cm^{-1} when the imidazole is deprotonated.[35] The orientation of the imidazole ring relative to the Fe−N(pyrrole) axes is another factor that influences the ν(Fe−His) stretch.[36−38] When the histidine ring is collinear with an axis along two heme meso-carbons, the ν(Fe−His) is observed ∼20 cm^{-1} lower than when the histidine ring is oriented along a N−Fe−N (pyrrole) axis. Thus, the identical ν(Fe−His) observed in *nm*-HO and *pa*-HO demonstrate that in both proteins the heme iron is bound to a proximal histidine with similar electronegativity and orientation with respect to the Fe−N(pyrrole) axes. The recent X-ray structure of *nm*-HO showed that, as in HO-1, the proximal histidine is engaged in a hydrogen-bonding interaction with a carboxylate side chain and that the imidazole ring is oriented along the heme β−δ-meso-axis.[12] In *pa*-HO, the proximal histidine is likely to adopt a similar orientation and to be hydrogen-bonded to Glu-30, in a manner homologous to Glu-29 in h-HO1. No significant perturbation of these structural parameters appears to take place in the Asn-19 Tyr/Phe-117 Tyr double mutant of *pa*-HO, since the ν(Fe−His) is only 2 cm^{-1} lower than in the wild-type protein. In contrast to the conserved ν(Fe−His) observed in all three heme protein complexes, significant variations are observed in the 350−450 cm^{-1} region, where bending modes of the peripheral propionate and vinyl groups occur.[39] These changes reveal differences in the configurations of the heme peripheral groups that are particularly worth pointing out when comparing the wild-type and double mutant *pa*-HO, because the Asn-19 Lys/Phe-117 Tyr mutations are aimed at changing the interactions experienced by the heme propionate groups.

Table 2. Regioselectivity of Heme Oxygenation

	biliverdin isomer ratio (%)[a]			
pa-HO	α	β	δ	γ
wt	0	30	70	0
Asn-19 Lys	0	30	70	0
Phe-117 Tyr	0	30	70	0
Asn-19 Lys/Phe-117 Tyr	55	10	35	0

[a] The percentage of each isomer was obtained by integration of the peaks within each chromatogram. The reported values are an average obtained from five separate experiments. The standard deviation is ±5%

Catalytic Turnover of the *pa*-HO Mutants. As previously reported for the wild-type *pa*-HO, the NADPH cytochrome P450 reductase catalyzed reaction yields ferric Fe^{III}−biliverdin as the product of the reaction (data not shown).[8] Extraction of biliverdin from the reaction mixture, followed by esterification of the propionate groups and separation of the different isomers by HPLC, indicates the formation of δ-biliverdin (70%) and β-biliverdin (30%) (Table 2). As will be detailed below, the β-biliverdin isomer is formed from oxidation of the minor (m) heme orientational isomer, related to the major isomer (M) by 180° rotation of the heme along the α−γ-axis, which places the β-meso-carbon of m in the site normally occupied by the δ-meso-carbon of M. Catalytic turnover of the single mutants Asn-19 to Lys and Phe-117 to Tyr, in the presence of NADPH cytochrome P450 reductase shows no change in regioselectivity (Table 2). In contrast, analysis of the products obtained from the reaction catalyzed by the *pa*-HO double mutant (Asn-19 Lys/Phe-117 Tyr) indicates a significant change in the regioselectivity of the reaction, as is evident from the formation of α-biliverdin (55%), δ-biliverdin (35%), and β-biliverdin (10%). The NMR studies outlined below demonstrate that the formation of α-biliverdin is a consequence of a dynamic equilibrium of two heme seatings in the double mutant.

Resonance Assignments for Cyanide-Inhibited Wild-Type *pa*-HO and *cd*-HO. In addition to the difficulties inherent in obtaining NMR spectra of short-lived, paramagnetically affected signals, the assignment of resonances corresponding to the heme active site of ferric hemoproteins is typically met with challenges imposed by heme isomerism, which results in the virtual

(33) Sun, J.; Wilks, A.; Ortiz de Montellano, P. R.; Loehr, T. M. *Biochemistry* **1993**, *32*, 14151−14157.
(34) Wilks, A.; Moënne-Loccoz, P. *J. Biol. Chem.* **2000**, *275*, 11686−11692.
(35) Kitagawa, T., Spiro, T. G., Ed.; John Wiley & Sons: New York, 1988; Vol. 3, pp 97−131.
(36) Bangcharoenpaurpong, O.; Schomacker, K. T.; Champion, P. M. *J. Am. Chem. Soc.* **1984**, *106*, 5688−5698.
(37) Smulevich, G.; Feis, A.; Focardi, C.; Tams, J.; Welinder, K. G. *Biochemistry* **1994**, *33*, 15425−15432.
(38) Othman, S.; Richaud, P.; Verméglio, A.; Debois, A. *Biochemistry* **1996**, *35*, 9224−9234.
(39) Hu, S.; Smith, K. M.; Spiro, T. G. *J. Am. Chem. Soc.* **1996**, *118*, 12638−12646.

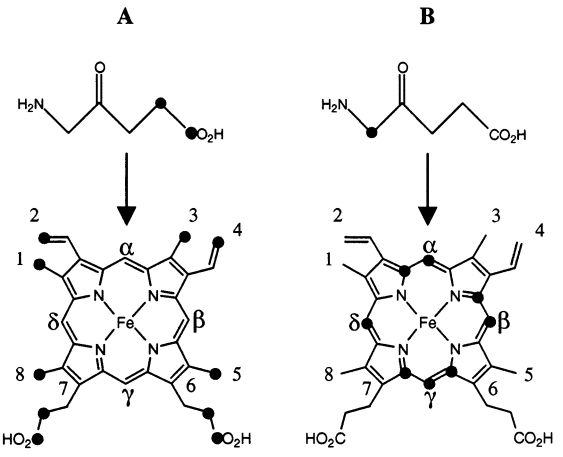

Figure 3. (A) ^{13}C-Labeling pattern obtained when protoporphyrin IX is biosynthesized from [1,2-^{13}C]ALA and (B) ^{13}C-labeling pattern obtained from [5-^{13}C]ALA. (●) Positions labeled with ^{13}C. For details, see refs 24 and 27.

doubling of resonances originating from the macrocycle.[40,41] Further complication arises from the asymmetric distribution of unpaired electron density on the heme macrocycle, which is manifested in large isotropic shifts for some nuclei and negligible ones for others.[42−44] To circumvent these problems, we have devised a biosynthetic method for the isotopic labeling of protoheme IX (heme), which can be used to introduce ^{13}C to virtually any position in the macrocycle.[24] The availability of hemoproteins reconstituted with ^{13}C-labeled heme facilitates the resonance assignment process, as has been demonstrated by the complete assignment of ^{1}H and ^{13}C resonances in both heme orientational isomers of mitochondrial cytochrome b_5.[27] As will be shown below, unambiguous ^{1}H and ^{13}C assignments of resonances originating from the heme active site of wild-type and mutant heme oxygenases have been obtained by utilizing enzymes reconstituted with ^{13}C-labeled heme. The assignment of heme resonances can be largely facilitated by judiciously labeling the heme macrocycle; this can be accomplished by carefully positioning the ^{13}C label in the heme precursors utilized in the biosynthesis of labeled heme. We used [1,2-^{13}C]-δ-aminolevulinic acid ([1,2-^{13}C]ALA) as a heme precursor for the preparation of heme labeled at the four methyl, two vinyl-β, and carbonyl carbons[24,27] (Figure 3A), and [5-^{13}C]ALA was used to prepare heme labeled at the meso-carbons (Figure 3B). The low-frequency portion of the 1-D ^{13}C NMR spectrum (^{1}H-coupled) obtained from wild-type *pa*-HO reconstituted with heme labeled from [1,2-^{13}C]ALA clearly shows that the heme methyl groups (quartets) resonate between −10 and −70 ppm (Figure 4A). More than four methyl signals are observed in the spectrum because wild-type *pa*-HO exists in solution as a mixture of two heme orientational isomers, coexisting in a 70:30 ratio of major to minor isomer (M:m = 70:30). In fact, the HMQC spectrum reveals the presence of eight heterocorrelations in this region, which permit the identification of ^{1}H resonances originating from heme methyl groups in the major and minor heme orientational isomers. The assignments described below will only be concerned with resonances originating from the major isomer. The high-frequency portion of the ^{13}C spectrum in Figure 4B shows that the vinyl-β carbons (triplets) and carbonyl carbons (doublets) resonate between 190 and 140 ppm, and the heterocorrelations seen in the HMQC spectrum identify the corresponding vinyl-β protons. The doublets ($^{1}J_{CC} \sim 55$ Hz) originating from each of the propionate carbonyl carbons are a consequence of the fact that the ^{13}C-labeled carbonyl carbons are attached to a ^{13}C-labeled β-propionate (see Figure 3A). In fact, this feature of the labeling pattern also permits the unambiguous identification of the β-propionate carbons, because the corresponding resonances are triplets ($^{1}J_{CH} \sim 140$ Hz) of doublets ($^{1}J_{CC} \sim 55$ Hz) (data not shown); the corresponding β-propionate proton resonances are thus readily identified via heteronuclear HMQC correlations. It is therefore evident that the use of *pa*-HO reconstituted with heme labeled as shown in Figure 3A permits the relatively straightforward identification of ^{1}H and ^{13}C resonances originating from all heme methyl, vinyl-β, and propionate-β groups. It is also readily apparent that the utilization of ^{13}C-labeled heme is especially useful in the unambiguous identification of ^{1}H resonances that are buried under the intense envelope of diamagnetic resonances.

The next step in the assignment strategy entails correlating these resonances with the aid of a WEFT−NOESY spectrum after a suitable entry point has been identified. In this context, the labeling pattern of Figure 3B is not only useful to identify the ^{1}H and ^{13}C resonances corresponding to the heme meso-positions, but it also provides a suitable entry point for the interpretation of NOESY cross correlations. Figure 5 depicts the 1-D ^{13}C NMR spectrum obtained from *pa*-HO reconstituted with heme labeled as in Figure 3B. This spectrum exhibits intense resonances at 84.8, 74.5, and −15.2 ppm devoid of HMQC correlations, which clearly indicates that these resonances must originate from the quaternary pyrrole-α carbons in the major isomer. In addition, the HMQC spectrum of Figure 5 reveals that four intense ^{13}C resonances (42.46, 28.24, 6.47, −0.92 ppm) exhibit heterocorrelations; these resonances must therefore originate from meso-carbons in the major isomer. Close inspection of the 1-D ^{13}C NMR spectrum of Figure 5 reveals that three of the meso-carbon resonances (28.24, 6.47, and −0.92 ppm) are affected by $^{1}J_{CC}$ coupling, whereas the fourth (42.46 ppm) is not. This observation indicates that the resonance at 42.46 ppm arises from meso-carbon δ because this is the only meso-carbon that is not attached to a labeled pyrrole-α carbon (see Figure 3B). The uniqueness of meso-carbon δ, which is conferred by the labeling pattern, makes this position an ideal entry point to interpret the NOESY cross correlations. Furthermore, NOESY cross correlations identifying heme resonances buried under the large envelope of diamagnetic resonances can be readily validated if they match the ^{1}H chemical shifts obtained from HMQC data.

As indicated above, the carbon resonance corresponding to meso-C_δ facilitates the identification of meso-H_δ and provides a unique entry point for the interpretation of NOESY spectra. Thus, a WEFT−NOESY spectrum (Figure 6) reveals a correlation between meso-H_δ (−2.51 ppm) and heme methyl 1 (1-Me) at 22.69 ppm, which in turn is correlated to vinyl-β proton 2 ($2V_\beta$) at −0.80 ppm. Both $2V_\beta$ protons (−0.80 and −1.35

(40) Keller, R. M.; Wüthrich, K. *Biochim. Biophys. Acta* **1980**, *621*, 204−217.
(41) La Mar, G. N. *Proc. Natl. Acad. Sci. U.S.A.* **1978**, *75*, 5755−5759.
(42) La Mar, G. N.; S., d. R. J. In *Biological Magnetic Resonance*; Berliner, L. J., Reuben, J., Eds.; Plenum: New York, 1993; Vol. 12, pp 1−78.
(43) Banci, L. In *Biological Magnetic Resonance*; Berliner, L. J., Reuben, J., Eds.; Plenum: New York, 1993; Vol. 12, pp 79−112.
(44) Satterlee, J. D.; Alam, S.; Yi, Q.; Erman, J. E.; Constantinidis, I.; Russell, D. J.; Moench, S. J. In *Biological Magnetic Resonance*; Berliner, L. J., Reuben, J., Eds.; Plenum: New York, 1993; Vol. 12, pp 275−297.

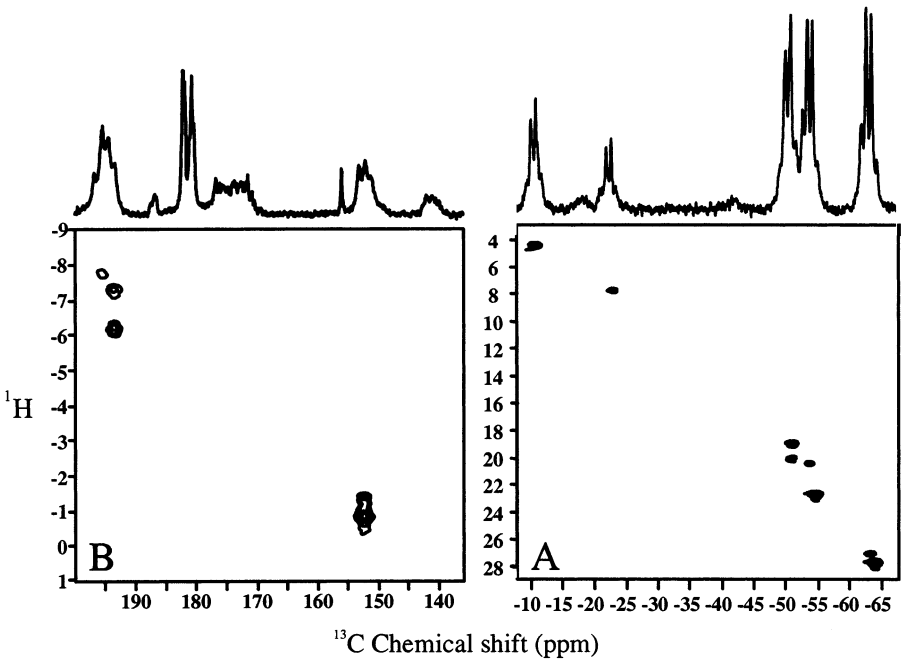

Figure 4. Low (A) and high (B) frequency (^{13}C) portions of the HMQC spectrum of wild-type *pa*-HO−CN reconstituted with heme derived from [1,2-^{13}C]ALA (see Figure 3A) showing both contour plot and 1-D ^{13}C spectrum.

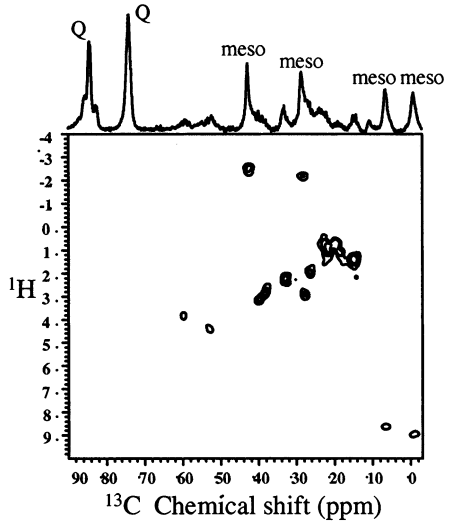

Figure 5. Portion of the HMQC spectrum of wild-type *pa*-HO−CN reconstituted with heme derived from [5-^{13}C]ALA (see Figure 3B) showing both contour plot and 1-D ^{13}C spectrum. Peaks in the 1−D ^{13}C spectrum labeled Q originate from porphyrin quaternary carbons.

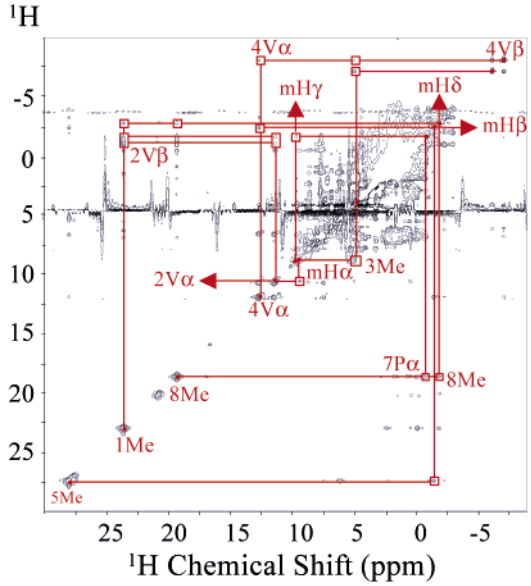

Figure 6. WEFT−NOESY of *pa*-HO reconstituted with heme derived from [5-^{13}C]ALA.

ppm) are correlated to the 2Vα proton at 10.74 ppm; the latter is correlated to the meso-H$_\alpha$ proton at 8.63 ppm and this meso-hydrogen is correlated to the 3-Me proton at 4.41 ppm, which in turn, is correlated to 4V$_\beta$ protons at −7.02 and − 7.97 ppm. One of the 4V$_\beta$ protons (−7.97 ppm) is correlated to the 4V$_\alpha$ proton (12.06 ppm) and this is correlated to the meso-H$_\beta$ proton (−2.20 ppm), which can be correlated to the 5-Me protons at 27.71 ppm. The assignments obtained for *pa*-HO are summarized in Table 3.

The assignments for *cd*-HO (Table 3) were carried out in a manner similar to that described above for *pa*-HO. In brief, a 1-D proton-coupled ^{13}C NMR spectrum obtained with *cd*-HO reconstituted with heme labeled as in Figure 3A allowed us to identify the ^{13}C resonance frequencies corresponding to heme methyl, β-propionates, and β-vinyl groups; the corresponding ^{1}H resonances were obtained from the HMQC spectrum in Figure S2. Enzyme reconstituted with heme labeled as in Figure 3B was used to identify the resonances arising from meso-carbons and meso-hydrogens with the aid of the HMQC map of Figure S3, and the WEFT−NOESY map of Figure S4 permitted the assignment of these resonances to the corresponding heme groups, as described above for *pa*-HO.

Interpretive Model for the NMR Spectroscopic Studies. The influence of the geometry and nature of axial ligands on the properties of low-spin ferric porphyrins and hemoproteins is well-known. For instance, it has been known for quite some time that the orientation of planar axial ligands exerts a large influence on the spread of the methyl resonances originating from low-spin ferric heme in hemoproteins, as well as in low-

Table 3. ^{1}H and ^{13}C NMR Chemical Shifts for the Cyanide Complexes of *pa*-HO and *cd*-HO

	pa-HO (10 °C)		*cd*-HO (35 °C)	
position	^{1}H (ppm)	^{13}C (ppm)	^{1}H (ppm)	^{13}C (ppm)
1-Me	22.69	−55.32	5.44	−13.14
3-Me	4.41	−11.10	19.18	−42.52
5-Me	27.71	−64.44	8.52	−20.06
8-Me	19.01	−51.45	10.59	−22.88
2-Vα	10.74	76.23	15.73	
2-Vβ	−0.80, −1.35	152.38	−3.69, −4.09	182.67
4-Vα	12.06	31.11	10.10	
4-Vβ	−7.02, −7.97	193.59	1.70, 1.28	147.08
meso-α	8.63	6.47	−2.58	58.58
meso-β	−2.20	28.24	8.19	18.75
meso-γ	8.95	−0.92	2.42	33.27
meso-δ	−2.51	42.46	7.78	21.73
6-P-α	6.33	−14.5		
6-P-β			0.91, −0.15	130.42
7-P-α	−1.20	−1.64		
7-P-β			−0.28, −0.58	113.93

spin Fe^{III} porphyrinates.[45−47] The fundamental property that allows this mechanism to operate is the interaction of the proximal histidine with the iron-centered e-symmetry d orbitals, which in turn individually interact with porphyrin 3e(π) orbitals to reduce their degeneracy. The end result is the destabilization of one member of the porphyrin 3e(π) orbitals and the stabilization of another, hence leading to an uneven distribution of electron spin density among the four pyrrole rings in the porphyrin.[45,48] More recently, the concept of counter-rotation of the g or χ tensor with rotation of axial ligand planes away from one of the N−Fe−N axes in the heme has been used to predict the orientation of the in-plane magnetic axis utilizing ^{13}C NMR[49−53] and ^{1}H NMR[54,55] spectroscopic data. Shokhirev and Walker carried out Hückel calculations of the effect of axial ligand nodal plane orientation, assuming counter-rotation of the g tensor, to produce heme methyl shifts that provide consistent predictions of the order and magnitude of observed methyl shifts for a large number of hemoproteins.[55]

Figure 7 depicts schematically the orientation of the proximal histidine−imidazole plane projected onto the heme ring, where the imidazole plane forms an angle ϕ of 135° with the molecular x-axis, which is aligned along the nitrogen atoms of heme pyrrole rings II and IV.[55] Consequently, the molecular z-axis is aligned along the heme normal, and the molecular y-axis is aligned along the nitrogen atoms of pyrrole rings I and III. The plot shown in Figure 7, which is adapted from a plot summarizing the Hückel calculations performed by Shokhirev and Walker,[55] shows the isotropic shift patterns predicted for heme methyl groups 1, 3, 5, and 8 as a funcion of the angle ϕ formed between the axial ligand plane and the molecular x-axis. From the plot in Figure 7 it is possible to predict that for a histidine−imidazole plane angle of 178°, which corresponds to the orientation of the proximal histidine−imidazole plane in the X-ray crystal structure of sperm-whale myoglobin,[56] the heme-methyl isotropic shifts obtained experimentally for the cyano complex of sperm whale myoglobin[57] are 5-Me > 1-Me > 8-Me > 3-Me (27.0, 18.6, 12.9, 4.8 ppm). It is evident that the order of methyl resonances is correctly predicted and that the predicted shifts are acceptable. In a similar manner, Shokhirev and Walker utilized the predictive power of the plot in Figure 7 to correctly suggest an angle ϕ of 125° for the proximal imidazole plane of h-HO-1, on the basis of NMR assignments reported by La Mar and co-workers.[58,59] These assignments demonstrated that the order of chemical shifts in cyanide-inhibited h-HO-1 is 3-Me > 8-Me > 5-Me > 1-Me (19.6, 10.5, 9.0, 4.9), which in the context of the plot shown in Figure 7 suggest an angle ϕ of 130°, a value that was corroborated by the X-ray crystal structure of h-HO-1[13] and r-HO-1.[15] Similar types of comparisons carried out with many heme-containing proteins clearly demonstrated the importance of axial ligand plane orientation on the observed proton shifts.[55] Consequently, the calculations of Shokhirev and Walker provide a predictive framework to study hemoproteins for which a structure has not yet been obtained. In this work, we have made use of the predictive power of these calculations to estimate the angle of the histidine−imidazole plane in *cd*-HO, *pa*-HO, and site-directed mutants of *pa*-HO.

The Orientation of the Histidine Plane in *pa*-HO Is Different Than That of Other Known Mammalian and Bacterial Heme Oxygenases. The high-frequency portion of the ^{1}H NMR spectrum of *cd*-HO (Figure 8a) is almost identical to that reported for r-HO-1[58] and h-HO1,[59] in that there is only one methyl resonance resolved from the diamagnetic envelope. The ^{1}H resonance assignments summarized in Table 3 indicate that the order of heme methyl resonances is 3-Me > 8-Me > 5-Me > 1-Me (19.05, 10.45, 8.39, 5.30 ppm), which in the context of the calculations summarized in Figure 7 strongly suggests that the proximal histidine−imidazole plane in *cd*-HO forms an angle of approximately 130° with the molecular x-axis and is nearly parallel to the heme $\beta-\delta$-meso-axis. In comparison, the resolved portion of the ^{1}H NMR spectrum of *pa*-HO (Figure 8b), displays three resolved methyl resonances originating from the major isomer and is clearly distinct from those corresponding to *cd*-HO, r-HO-1, and h-HO-1. This feature of the ^{1}H spectrum strongly suggests that the histidine−imidazole plane in *pa*-HO is oriented at an angle ϕ that is different from the 130° typically observed in all other heme oxygenases for which this information is available. In fact, the ^{1}H resonance assignments of Table 3 indicate that the order of heme methyl resonances obtained from *pa*-HO is 5-Me > 1-Me > 8-Me> 3-Me (27.71, 22.69, 19.01, 4.41 ppm); consequently, the plot of Figure 7 predicts that the proximal histidine−imidazole plane forms an angle ϕ of ∼35° with the molecular x axis and is aligned almost parallel to the heme α−γ-meso-axis. It is interesting to note that in *pa*-HO, which forms β- and δ-biliverdin, the histidine−imidazole plane is oriented along the α−γ-

(45) Walker, F. A. *J. Am. Chem. Soc.* **1980**, *102*, 3254−3256.
(46) Goff, H. *J. Am. Chem. Soc.* **1980**, *102*, 3252−3254.
(47) Satterlee, J. D. *Annu. Rep. Nucl. Magn. Reson. Spectrosc.* **1986**, *17*, 79−178.
(48) Walker, F. A.; Buehler, J.; West, J. T.; Hinds, J. L. *J. Am. Chem. Soc.* **1983**, *105*, 6923−6929.
(49) Turner, D. L.; Salgueiro, C. A.; Schenkels, P.; LeGall, J.; Xavier, A. V. *Biochim. Biophys. Acta* **1995**, *1246*, 24−28.
(50) Turner, D. L. *Eur. J. Biochem.* **1993**, *211*, 563−568.
(51) Banci, L.; Pierattelli, R.; Turner, D. L. *Eur. J. Biochem.* **1995**, *232*, 522−527.
(52) Pierattelli, R.; Turner, D. L. *Eur. Biophys. J.* **1996**, *24*, 342−347.
(53) Louro, R. O.; Correia, I. J.; Brennan, L.; Coutinho, I. B.; Xavier, A. V.; Turner, D. L. *J. Am. Chem. Soc.* **1998**, *120*, 13240−13247.
(54) Shokhirev, N. V.; Walker, F. A. *J. Am. Chem. Soc.* **1998**, *120*, 981−990.
(55) Shokhirev, N. V.; Walker, F. A. *JBIC* **1998**, 581−594.
(56) Quillin, M. L.; Tiansheng, L.; Olson, J. S.; Phillips, G. N.; Dou, Y.; Ikeda-Saito, M.; Regan, R.; Carlson, M.; Gibson, Q. H.; Li, H.; Elber, R. *J. Mol. Biol.* **1995**, *245*, 416−436.
(57) Emerson, S. D.; La Mar, G. N. *Biochemistry* **1990**, *29*, 1545−1556.
(58) Hernandez, G.; Wilks, A.; Paolesse, R.; Smith, K. M.; Ortiz de Montellano, P. R.; La Mar, G. N. *Biochemistry* **1994**, *33*, 6631−6641.
(59) Gorst, C. M.; Wilks, A.; Yeh, D. C.; Ortiz de Montellano, P. R.; La Mar, G. N. *J. Am. Chem. Soc.* **1998**, *120*, 8875−8884.

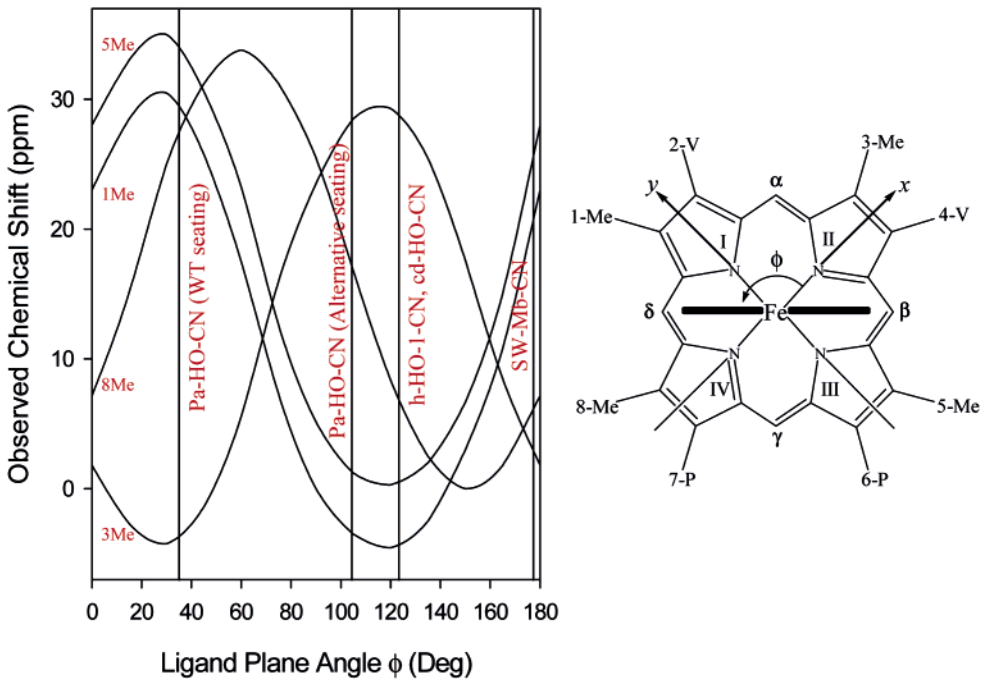

Figure 7. (Right) Right-handed coordinate system and nomenclature used for describing the projection of the His−imidazole plane onto the porphyrin ring. The *x*-axis is aligned along the nitrogen atoms of pyrrole rings II and IV of the heme, the *y*-axis is along the nitrogen atoms of pyrrole rings I and III, and the *z*-axis is normal to the heme. (Left) Dependence of observed heme-methyl shifts on the angle ϕ formed between the molecular *x*-axis and the projection of the imidazole plane. Adapted from Figure 5 in ref 55.

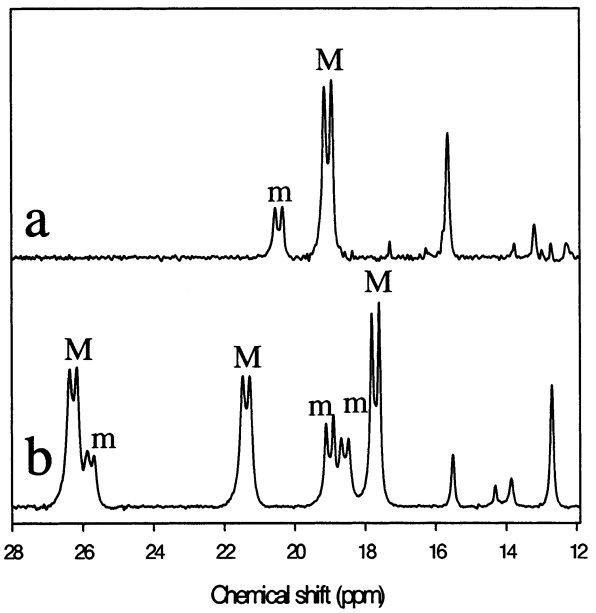

Figure 8. High-frequency portion of the ^{1}H NMR spectra of (a) *cd*-HO−CN and (b) *pa*-HO−CN reconstituted with heme derived from [1,2-^{13}C]-ALA. The $^1J_{CH}$ doublets originate from methyl groups in the major (M) and minor (m) heme orientational isomers.

meso-axis, whereas in r-HO-1, h-HO-1, and *cd*-HO, which form α-biliverdin, the histidine−imidazole plane is oriented along the $\beta-\delta$-meso-axis. The orientations of the heme imidazole planes in wild-type *pa*-HO and *cd*-HO are consistent with the fact that both proteins display identical ν(Fe−His) at 222 cm^{-1}, since this stretching vibration is insensitive to the meso-axis ($\alpha-\gamma$ or $\beta-\delta$) that is collinear with the imidazole plane.

A Dynamic Exchange between Two Heme Seatings in Asn-19 Lys/Phe-117 Tyr *pa*-HO Is Responsible for the Altered Regioselectivity of the Double Mutant. The crystal structures of *N. meningitidis* heme oxygenase (*nm*-HO)[12] and h-HO-1[13] revealed that conserved residues Lys-16 and Tyr-112 in *nm*-HO interact with the heme propionates. By comparison, the amino acid sequence of *pa*-HO, in the context of the three-dimensional structure of *nm*-HO, indicates that these residues in *pa*-HO are Asn-19 and Phe-117, respectively. This observation suggested to us that the unique value of the angle ϕ formed between the histidine−imidazole plane and the molecular *x*-axis, as well as the unique regioselectivity exhibited by *pa*-HO (β- and δ-biliverdin), might be related to different interactions between the heme propionates and the polypeptide, which presumably promote an alternative heme seating that is conducive to β- and δ-meso-hydroxylation. This hypothesis was tested with the Asn-19 Lys/Phe-117 Tyr mutant, which was constructed with the aim of restoring the hydrogen bonding and ionic interactions observed between the heme propionates and these residues in h-HO-1, r-HO-1, and *nm*-HO. The double mutant was found to hydroxylate the heme at the δ- (35%), β- (10%), and α-meso (55%) positions. It will be shown below that this unusual pattern of regioselectivity is indeed a consequence of perturbing the microenvironment of the heme propionates, which results in the stabilization of two heme seatings related to one another by a 110° in-plane rotation of the heme.

The resolved portion of the ^{1}H NMR spectrum of Asn-19 Lys/Phe-117 Tyr *pa*-HO at 35 °C (Figure 9a) displays broad and almost featureless peaks; however, as the temperature is lowered, the peaks become gradually sharper and new peaks emerge. Below 15 °C, the shape of the spectra no longer changes, except for the expected temperature-dependent shifts that are typical of paramagnetically affected resonances.[47] A striking characteristic of the ^{1}H NMR spectrum of the double mutant at 10 °C (Figure 9e) is the large number of resonances resolved from the diamagnetic envelope. The relative intensity

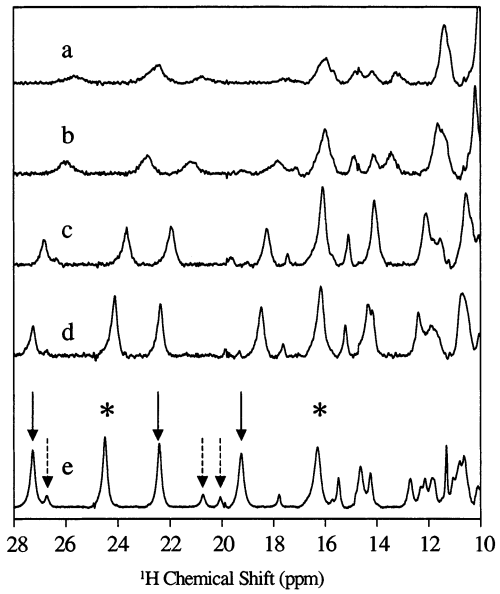

Figure 9. Variable-temperature ^{1}H NMR spectra of the Asn-19 Lys/Phe-117 Tyr double mutant of *pa*-HO−CN. Spectra were acquired at (a) 35, (b) 30, (c) 20, (d) 15, and (e) 10 °C. The solid arrows in plot e correspond to methyl resonances originating from the major orientational isomer exhibiting the wild-type seating, while dashed arrows highlight the corresponding minor isomer. Asterisks highlight two methyl resonances originating from the major orientational isomer displaying the alternative heme seating.

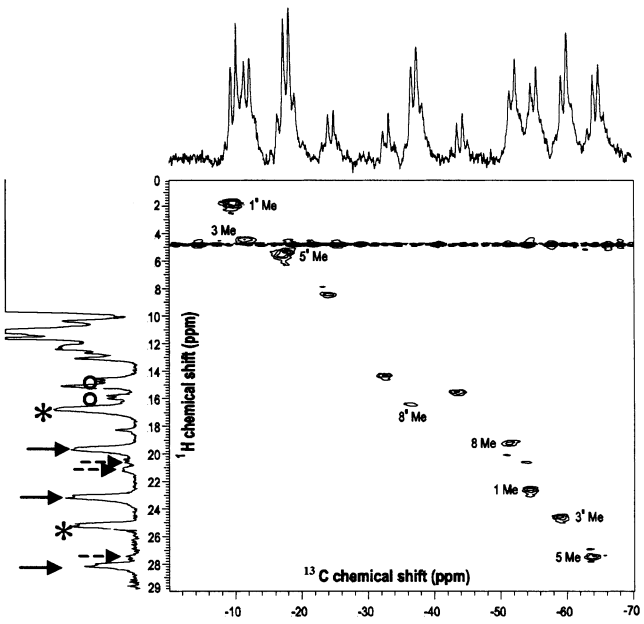

Figure 10. HMQC spectrum of the cyanide-inhibited Asn-19 Lys/Phe-117 Tyr *pa*-HO reconstituted with heme derived from [1,2-^{13}C]ALA. Only the low-frequency (^{13}C) region of the spectrum, which displays the heme methyl resonances, is shown. The 1-D ^{1}H and nondecoupled ^{13}C spectra are shown to illustrate the J_{CH} splitting. Arrows and dashed arrows, respectively, represent the major and minor orientational isomers exhibiting the wild-type heme seating. Asterisks and open circles, respectively, represent the major and minor isomers exhibiting the alternative heme seating.

of these resonances suggests that at least five of them are likely to originate from heme methyl groups. The large number of resonances originating from heme methyl groups suggests two possibilities: (a) the presence of two heme orientational isomers coexisting with almost identical concentrations or (b) two heme seatings exchanging with one another at a frequency that at 10 °C is slow relative to the NMR time scale but similar to it at 35 °C. Close inspection of the ^{1}H NMR spectrum of the Asn-19 Lys/Phe-117 Tyr double mutant at 10 °C (Figure 9e) allowed us to rule out the first possibility. In this spectrum, black arrows highlight those methyl resonances that are also observed in the ^{1}H NMR spectrum corresponding to the major isomer of WT *pa*-HO, and dashed arrows highlight the methyl resonances of the corresponding minor isomer. These observations, together with the temperature-induced changes in the NMR spectra, strongly suggest that the Asn-19 Lys/Phe-117 Tyr double mutant exists as a mixture of molecules harboring the heme in two distinct seatings. The two seatings, one of which is identical to the seating of the wild-type enzyme, are related to one another by chemical exchange. Furthermore, the spectrum obtained at 10 °C also demonstrates that each of the heme seatings exists as a mixture of two heme orientational isomers.

To probe the hypothesis suggesting that the resonances highlighted by arrows and asterisks in Figure 9e originate from heme methyl groups in two distinct heme seatings, the Asn-19 Lys/Phe-117 Tyr double mutant of *pa*-HO was reconstituted with heme labeled as in Figure 3A. The resolved portion of the ^{1}H NMR spectrum of the double mutant reconstituted with labeled heme (Figure 10) demonstrates that, as expected, those resonances with chemical shifts identical to the peaks originating from heme methyl groups in the major (solid arrows) and minor (dashed arrows) isomer of wild-type *pa*-HO exhibit ∼140 Hz $^1J_{CH}$ splitting. It is also apparent that the peaks labeled with an asterisk in Figure 9e and 10 are also split by a ∼140 Hz coupling constant, thus demonstrating that these peaks originate from heme methyl groups in the alternative heme seating. Furthermore, the ^{1}H NMR spectrum of Figure 10 also facilitates the identification of two heme resonances that originate from the minor heme orientational isomer in the alternative heme seating, as is evident from the $^1J_{CH} \sim 140$ Hz doublets highlighted by an open circle. Additional evidence in support of the hypothesis that the resonances highlighted with arrows and asterisks in Figure 9e correspond to heme methyl groups was obtained from 1-D ^{13}C (^{1}H-coupled) and HMQC spectra, because the ^{13}C NMR spectrum (Figure 10) permits the identification of $^1J_{CH} \sim 140$ Hz quartets, which can be correlated to the corresponding heme-methyl ^{1}H resonances by HMQC. In fact, the latter spectrum displays at least 15 resolved resonances originating from heme methyl groups, thus providing ample confirmatory evidence that the Asn-19 Lys/Phe-117 Tyr double mutant of *pa*-HO exists as a mixture of four different molecules: two different heme seatings create a set of two and heme isomerism creates a subset of two from each heme seating isoform.

The nature of the several isoforms of Asn-19 Lys/Phe-117 Tyr coexisting in solution having been established, we turned our attention to assign the heme methyl resonances originating from the heme in the alternative heme seating (major isomer). Since the two heme seatings are in slow exchange at 10 °C, we used exchange spectroscopy (EXSY)[31] to map out those resonances that are correlated by exchange; the data are summarized by the EXSY spectrum of Figure 11. In this spectrum the exchange cross-peaks can be identified readily because they are significantly more intense than the NOE cross-peaks. Thus, the exchange correlations of Figure 11 (summarized

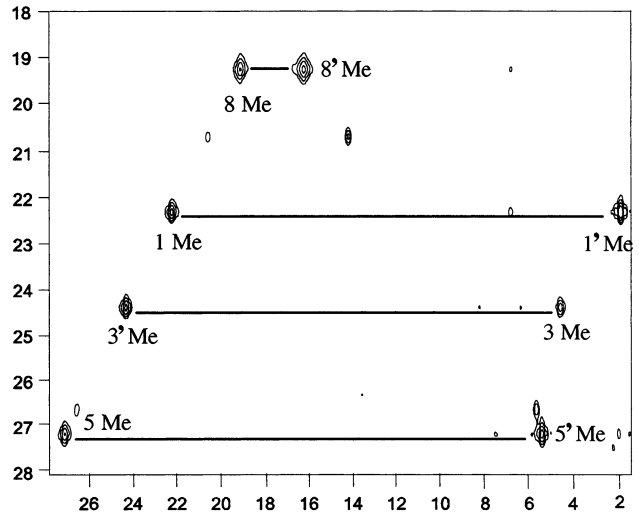

Figure 11. EXSY spectrum of the double mutant of *pa*-HO−CN. The heme methyl resonances arising from the wild-type and alternative heme seatings are labeled as 1, 3, 5, 8 and 1′, 3′, 5′, 8′, respectively.

below) allowed us to assign the resonances originating from methyl groups in the alternative heme seating.

wild-type seating		alternative seating
5-Me (27.71 ppm)	⇆	5′-Me (5.38 ppm)
1-Me (22.69 ppm)	⇆	1′-Me (1.74 ppm)
8-Me (19.01 ppm)	⇆	8′-Me (16.33 ppm)
3-Me (4.41 ppm)	⇆	3′-Me (24.55 ppm)

The assignments corresponding to heme methyl groups in the alternative heme seating reveal that the order of methyl shifts is 3′-Me > 8′-Me > 5′-Me > 1′-Me, therefore indicating that the proximal histidine−imidazole plane in the alternative heme seating of the Asn-19 Lys/Phe-117 Tyr mutant forms an angle ϕ of approximately 100° with the molecular *x*-axis (see Figure 7).

The orientation of the proximal histidine plane in the alternative heme seating, which is aligned along the nitrogen atoms of heme pyrrole rings II and IV, should result in a different ν(Fe−His) in the double mutant, relative to the wild-type protein. In the absence of other determinant factors, the alternative seating is expected to display a ν(Fe−His) above 222 cm^{-1}, possibly as high as 230 cm^{-1}.[36,37] However, the ν(Fe−His) observed in the double mutant protein is practically unchanged, at 220 cm^{-1}. Moreover, the relative intensity and bandwidth of the ν(Fe−His) are unaffected, thus giving no indication of multiple heme seatings within the substrate pocket of the double mutant. Good agreement between NMR and RR spectroscopic studies of this kind has been observed with globins and peroxidases, despite the fact that one technique (NMR) characterizes the 6cLS ferric cyano complex and the other the 5cHS ferrous heme. However, these systems were not in equilibrium between two seatings, as is the case of the *pa*-HO double mutant. It is therefore tempting to speculate that while the ferrous state favors a single heme seating, the ferric hydroperoxide (Fe^{III}−OOH) intermediate, which defines the regioselectivity, adopts both heme seatings observed by NMR spectroscopy.

In what follows, the dynamic equilibrium between the two heme seatings in the mutant enzyme will be analyzed in the context of the fold of *nm*-HO, which is typical of the fold

Scheme 1

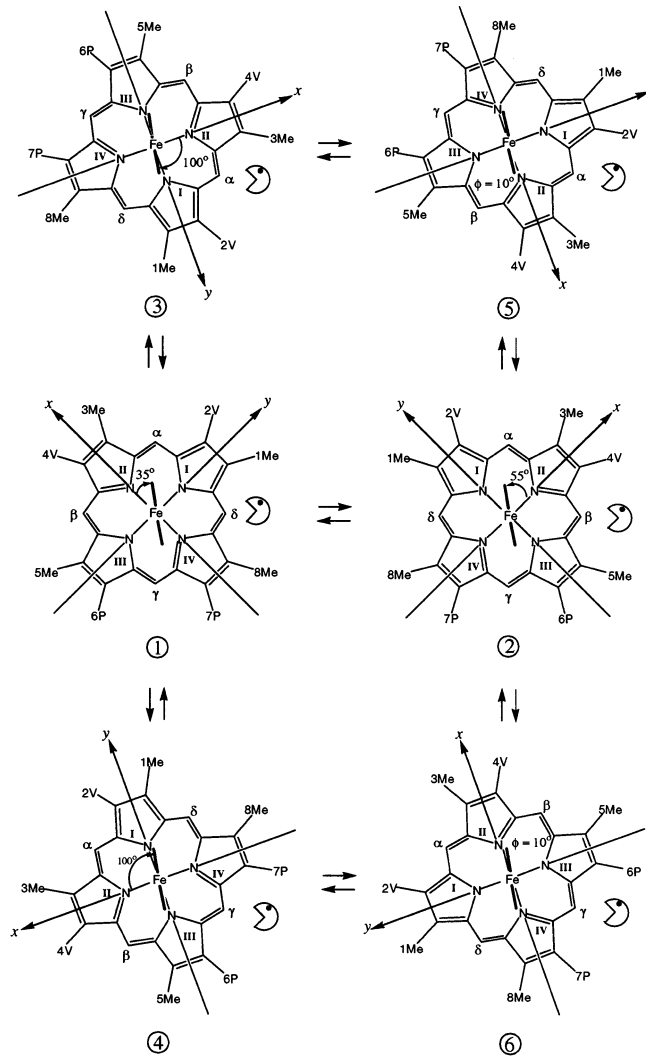

exhibited by heme oxygenases, and in the context of Scheme 1, assuming that the heme rotates in-plane, while the proximal histidine−imidazole plane remains in place. It is felt that an in-plane rotation of the heme is more likely than a rotation of the proximal histidine−imidazole plane, because the mutations that trigger the dynamic equilibrium described above are aimed at introducing hydrogen bonding and ionic interactions with the heme propionates; thus, it is likely that the in-plane heme rotation is a result of the heme propionates sampling two environments that stabilize these groups to approximately the same extent.

Until the recent discovery of *pa*-HO,[8] a trademark of heme oxygenases from a variety of different sources (h-HO-1, r-HO-1, *cd*-HO, and *nm*-HO) has been their ability to degrade heme with exquisite α-regioselectivity. Consequently, *pa*-HO is unusual among heme oxygenases in that it is the only known heme oxygenase that degrades heme to *δ*-biliverdin. The structures of h-HO-1[13] and r-HO-1[15] share a homologous, largely α-helical fold with the structure of the bacterial heme oxygenases (*nm*-HO[12] and *cd*-HO), despite the low sequence identity.[12] It is therefore not unreasonable to expect that the overall fold of *pa*-HO is likely to be similar to that of the heme oxygenases for which a structure is known, given the relatively high degree of sequence identity (37%) between *nm*-HO and *pa*-HO. In fact, assuming that the fold of *pa*-HO is typical of

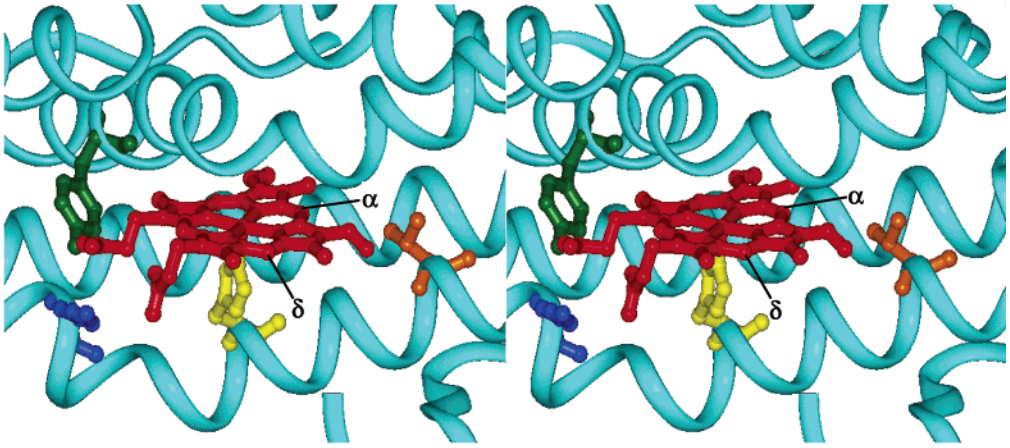

Figure 12. Stereoview of the heme-binding environment in *nm*-HO. The heme is red, the proximal His-23 is yellow, Tyr-112 is green, Lys-16 is blue, and Val-30 is orange. The α-meso-carbon, which is susceptible to attack in all α-hydroxylating heme oxygenases of known structure, is highlighted. PDB access code 1J77.

other heme oxygenases allowed us to conclude that Lys-16 and Tyr-112 in *nm*-HO (Lys-16 and Tyr-134 in h-HO-1), which form important hydrogen bonding and electrostatic interactions with the heme propionates, are replaced by Asn-19 and Phe-117 in *pa*-HO. Also, by assuming that the overall fold of *pa*-HO is typical of other heme oxygenases, the amino acid alignments allowed us to hypothesize that, in the absence of nearby residues capable of compensating for the lack of interactions between the heme propionates and Asn-19 and Phe-117 in *pa*-HO, replacing these residues for Lys and Tyr, respectively, would likely introduce the ionic and hydrogen-bonding interactions typically experienced by the heme propionates of other heme oxygenases. Consistent with this hypothesis, the heme in the *pa*-HO double mutant experiences a dynamic equilibrium between two heme seatings, which at 10 °C coexist with approximately equimolar concentrations. The fold of *nm*-HO (Figure 12) makes it evident that the heme seating of the enzyme orients the heme propionates such that they can interact with Lys-16 and Tyr-112; moreover, the heme seating results in the placement of the α-meso-carbon at the bottom of the heme pocket, where it is susceptible to hydroxylation, and the placement of the δ-meso-carbon at the exposed heme edge. It is also noteworthy that the 1.5-Å-resolution structure of *nm*-HO indicates that the predominant heme orientational isomer places pyrrole ring II and the β-meso-carbon at the deep end of the heme pocket,[12] an observation that is in agreement with our preliminary NMR spectroscopic investigations of *nm*-HO, which also indicate that one of the heme orientational isomers in this enzyme is largely predominant (M:m = 95:5; data not shown).

The phenomenon in which two heme seatings are related to one another by an in-plane rotation of the heme in the Asn-19 Lys/Phe-117 Tyr *pa*-HO can be summarized by the equilibria in Scheme 1. The scheme was constructed by placing the site of attack as is seen in the fold of *nm*-HO (see Figure 12) and by assuming that the major orientational isomer is the same as that favored by *nm*-HO. Results obtained from the NMR spectroscopic studies conducted with the Asn-19 Lys/Phe-117 Tyr *pa*-HO indicate that, in the major heme orientational isomer exhibiting the wild-type heme seating, the molecular *x*-axis forms an angle ϕ of 35° with the imidazole plane. This is illustrated by **1** in Scheme 1; consequently, the minor isomer exhibiting the wild-type seating (**2**) is obtained by rotating **1** 180° about the α−γ-meso-axis. Note that rotation of the heme about the α−γ-meso-axis only affects the macrocyle, leaving the axial ligand unperturbed, so in the minor isomer exhibiting the wild-type seating (**2**), the molecular *x*-axis makes an angle ϕ of 55° with the histidine−imidazole plane. The different value of ϕ in the major and minor isomers is consistent with the different patterns of resolved methyl resonances observed for the heme orientational isomers. The alternative heme seating corresponding to the major isomer can be obtained by considering that the NMR spectroscopic studies led us to conclude that the angle ϕ in the alternative heme seating is 100°. Thus, starting from the major isomer exhibiting the wild-type heme seating (**1**), it is possible to rotate the heme (hence, the *xy*-plane) 115° clockwise or 65° counterclockwise, to obtain **3** and **4**, respectively. The heme seating represented by **3** places the α-meso-carbon where it can be hydroxylated by the enzyme; hence, it is consistent with the regioselectivity of heme oxygenation exhibited by the Asn-19 Lys/Phe-116 Tyr double mutant of *pa*-HO, which we found produces α- (55%), δ- (35%), and β-biliverdin (10%). On the other hand, the heme seating represented by **4** places the γ-meso-carbon where it is susceptible to be hydroxylated in order to form γ-biliverdin. The fact that the double mutant enzyme does not oxidize heme to γ-biliverdin clearly indicates that the alternative heme seating displayed by the major isomer in the double mutant *pa*-HO is best represented by **3**. A similar analysis of the minor isomer is not possible, because the relatively low intensity of the corresponding resonances precluded their unambiguous assignment. However, if we assume that the minor isomer rotates in-plane in a manner that is similar to that described for the major isomer, it is possible to estimate the angle ϕ by rotating the major isomer displaying the alternative heme seating by 180° about the α−γ-meso-axis. In this manner, **5** and **6** are obtained by rotating **3** and **4**, respectively. It is apparent that **6** can be ruled out because it places the γ-meso-axis where it is susceptible for attack, while on the other hand, **5** is conducive to the formation of α-biliverdin. Consequently, it is possible to conclude that **1** and **2**, respectively, represent the major and minor heme orientational isomers in the wild-type seating, whereas **3** and **5**, respectively, represent the major and minor heme orientational isomers in the alternative heme seating.

Careful integration of ^{1}H NMR signals attributed to heme methyl groups in the major and minor isomers of molecules displaying the wild-type heme seating (**1** and **2**) accounts for

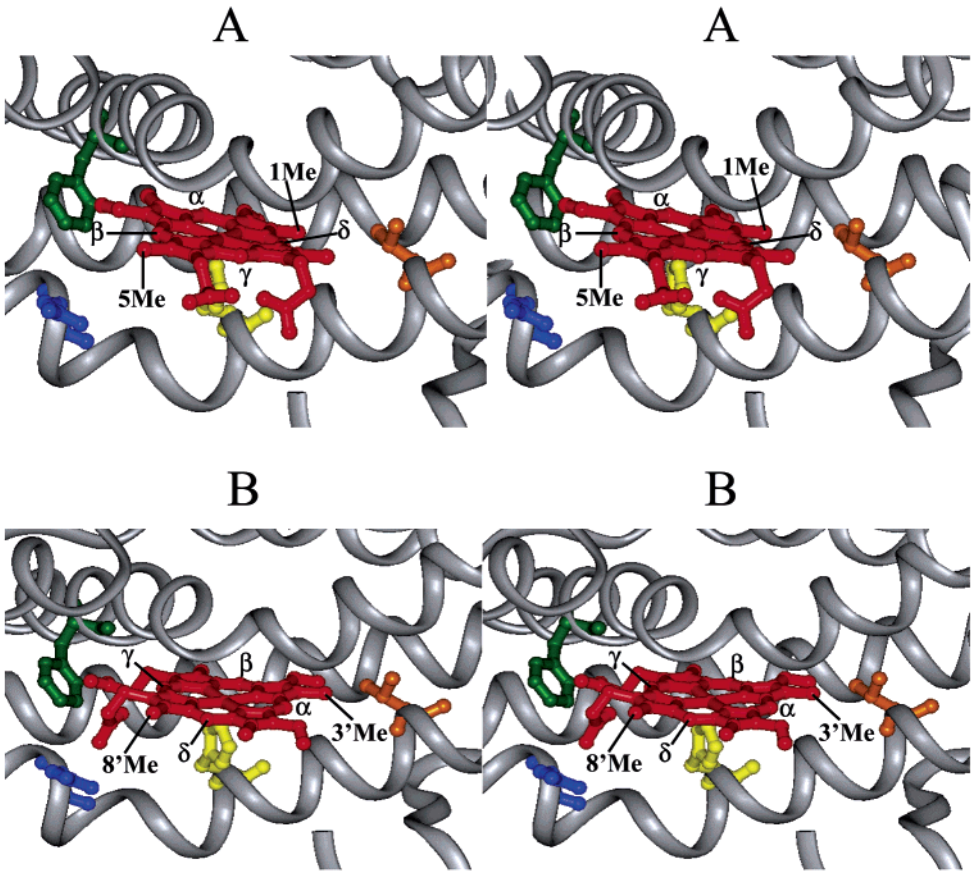

Figure 13. Stereoview of the predicted wild-type (A) and alternative (B) heme seatings in mutant *pa*-HO−CN, modeled into the fold of *nm*-HO, where the heme is shown in red, Lys-16 and Tyr-112 in *nm*-HO have been replaced by Asn-19 (blue) and Phe-117 (green). Val-30 in *nm*-HO (orange) is Val-33 in *pa*-HO. The wild-type seating of *pa*-HO (A) places the δ-meso-carbon where it is susceptible to hydroxylation, whereas 110° in-plane rotation of the heme results in the alternative seating (B), thus positioning the α-meso-carbon where it can be hydroxylated.

45% of the total concentration, whereas the remaining 55% corresponds to major and minor isomers in the alternative heme seating (**3** and **5**). The ^{1}H NMR spectrum also reveals that the ratio of heme orientational isomers (**1**:**2**) displaying the wild-type heme seating is 87:13. This implies that 39% of the molecules harbor heme where the angle ϕ is 35° (**1**), which is conducive to attack at the δ-meso-carbon, therefore explaining the formation of approximately 35% δ-biliverdin. The 87:13 ratio of major to minor orientational isomers displaying the wild-type heme seating also implies that approximately 6% of the molecules harbor a macrocycle that is rotated 180° about the α−γ-meso-axis (**2**). This rotation places the β-meso-carbon in a position that is susceptible for attack, therefore explaining the formation of approximately 10% β-biliverdin (Table 2). Biliverdin-α, on the other hand, is derived from the alternative heme seating depicted by **3**, which places the α-meso-carbon in a position where it is susceptible for attack. The ^{1}H NMR spectrum of the mutant reveals that the alternative heme seating, which accounts for 55% of the total concentration, is also heterogeneous in that two heme orientational isomers (**3**:**4** = 80:20) coexist. However, since 180° rotation of **3** about the α−γ-meso-axis results in **5** but does not exchange the position of meso-carbon α, it is apparent that only the α-meso-position is susceptible for attack, a prediction that is consistent with the experimental observations.

If **1** is incorporated into the fold of *nm*-HO, where Lys-16 and Tyr-112 have been replaced for Asn and Phe, respectively, a visual representation of the seating proposed for wild-type *pa*-HO is obtained (Figure 13A). This heme seating places the δ-meso-carbon in a position where it can be hydroxylated by the enzyme, and rotation of the heme about the α−γ-meso-axis places the β-meso-carbon where it is susceptible to hydroxylation; thus, the proposed heme seating for wild-type *pa*-HO is consistent with the characteristic δ- (70%) and β-regioselectivity (30%) displayed by the wild-type enzyme. Note that in the model displayed in Figure 13A, the imidazole plane is aligned nearly parallel with the α−γ-meso-axis and forms an angle ϕ of 35° with the molecular *x*-axis; the latter is aligned along the nitrogen atoms of pyrrole rings II (harboring 3-Me) and IV (harboring 8-Me). The heme propionates point in the direction of the exposed heme edge; hence, steric encumbrances between the relatively large (and charged) heme propionates and polypeptide residues are not anticipated. In a similar manner, a visual representation of the alternative heme seating in the Asn-19 Lys/Phe-117 Tyr double mutant of *pa*-HO can be modeled by inserting **3** into the fold of *nm*-HO (Figure 13B). It can be seen that the heme propionates interact with Lys-16 (Lys-19 in the double mutant) and Tyr 112 (Tyr-117 in the double mutant), and that the α-meso-carbon is placed at the bottom of the heme pocket, where it is observed in the structure of *nm*-HO. Also note that the imidazole plane is aligned nearly collinear with the N−Fe−N axis of pyrroles I and III and forms an angle ϕ of 110° with the molecular *x*-axis, which lies along the nitrogens of pyrrole ring II (harboring 3′-Me) and IV (harboring 8′-Me). As discussed above, the NMR spectroscopic studies carried out with the double mutant led us to

suggest that in the double mutant the heme seatings of Figure 13A,B are related by a dynamic 110° in-plane rotation of the heme. In fact, a NOESY spectrum of the Asn-19 Lys/Phe-117 Tyr double mutant reveals an NOE between a signal at −0.75 ppm and the resonances corresponding to 1-Me in the wild-type seating (Figure 13A) and 3′-Me in the alternative seating (Figure 13B). The signal at −0.75 ppm is tentatively attributed to one of the γ-methyl groups in Val-33 (Val 30 in *nm*-HO); hence, the NOE between this side chain resonance and the 1-Me and 3′-Me groups is consistent with the presence of two heme seatings, related by a 110° in-plane rotation of the heme.

Relevance to the Mechanism of Action of HO and Concluding Remarks. The discussion above suggests a strong contribution from steric interactions in the distal helix in dictating the regioselectivity of oxidative degradation; however, it is important to point out that electronic contributions are probably equally important but cannot be discerned from the data at hand. In this context, it is interesting to consider the results obtained from the oxidation of *meso*-methylhemes[16] and *meso*-formylhemes[17] by heme oxygenase. The γ-*meso*-methylheme was oxidized exclusively at the γ-meso-position, δ-*meso*-methylheme was oxidized at the δ- and α-meso-positions, and the β-derivative was found to be a poor substrate.[16] On the other hand, all four isomers of *meso*-formylheme are never oxidized at the meso-carbon bearing the electron-withdrawing formyl group.[17] These observations, which are not compatible with a simple steric steering of the iron-bound peroxide, suggest that the regioselectivity of heme oxygenation is also affected by the electronic structure of heme in heme oxygenase. Moreover, recent experiments carried out with heme models of the ferric hydroperoxide (Fe^{III}−OOH) complex of HO[18] suggest that the electronic structure of this key intermediate is crucial to the meso-hydroxylation of the heme in HO. These studies suggested that at ambient temperatures the electronic structure of this important ferric hydroperoxide intermediate is low-spin with the unpaired electron residing in a d_{xy} orbital. Work carried out with low-spin $(d_{xy})^1$ complexes has clearly demonstrated that in order to delocalize spin density from the d_{xy} orbital into the porphyrin π system, the macrocycle has to ruffle significantly, so that the nodal planes of the p_z orbitals of the macrocycle are no longer in the *xy*-plane and the components (projections) of these p_z orbitals in the *xy*-plane have the proper symmetry to interact with the d_{xy} orbital.[60] The porphyrin orbital with the right symmetry to interact with the ruffled macrocycle ($3a_{2u}\pi$) possesses large electron density at the meso-carbons;[18,61,62] therefore, it has been proposed that the large spin density at the meso-carbons directs the attack of the Fe^{III}−OOH intermediate on a heme meso-carbon.[18] If the porphyrin ring of the Fe^{III}−OOH intermediate is ruffled by virtue of its $(d_{xy})^1$ electronic structure, it is expected to place pairs of meso-carbons, i.e. α/γ and β/δ, approximately 0.6 Å above and below the heme plane,[60−62] where one will be susceptible to attack by the coordinated peroxide. Consequently, exclusive attack of the α-meso-carbon can only be explained if the γ-meso-carbon is shielded from attack by steric protection, strongly suggesting that the outcome of heme oxygenation is governed by an interplay between electronic and steric contributions.

Finally, it is also interesting to point out that the plane of the proximal histidine in *pa*-HO, which hydroxylates the β-meso-carbon, is aligned along the $\alpha-\gamma$-meso-axis, whereas the proximal histidine−imidazole plane in all other heme oxygenases (α-meso-hydroxylation) is aligned along the $\beta-\delta$-meso-axis. The data in Table 3 reveal that the meso-protons that lie on an axis that is perpendicular to the axis of the proximal ligand plane exhibit large isotropic shifts. For instance, meso-H_β and meso-H_δ in *pa*-HO exhibit chemical shifts of −2.2 and −2.5 ppm, whereas meso-H_α and meso-H_γ in *cd*-HO, *r*-HO-1,[59] and h-HO-1[58] exhibit similar shifts. Thus, a relatively large amount of unpaired electron density appears to reside at the meso-hydrogens located along an axis that is perpendicular to that of the proximal ligand plane and might suggest a potential link between the regioselectivity of oxidative cleavage and the orientation of the proximal histidine−imidazole plane. This potential correlation between regioselectivity and orientation of the proximal ligand, however, is not observed in the Asn-19 Lys/Phe-117 Tyr mutant of *pa*-HO−CN, where the alternative heme seating, which conduces to the formation of 55% α-biliverdin, is likely to display a proximal histidine−imidazole plane that is oriented nearly parallel to the axis along the nitrogen atoms of pyrrole rings I and III (Figure 13B). It is also important to point out that the cyanide complex of HO may not be the best system to study the effects of electronic structure on the reactivity and regioselectivity of the heme oxygenation reaction, because the cyanide complexes of HO exhibit a $(d_{xy})^2(d_{xz},d_{yz})^3$ electronic configuration, with the unpaired electron residing in one of the d_π ortitals, d_{xz} or d_{yz}. Iron(III) porphyrinates exhibiting an unpaired electron in one of the d_π orbitals have been shown to possess small to negligible unpaired electron density at the meso-carbons.[61,62] On the other hand, magnetic resonance studies conducted with models of the Fe^{III}−OOH complex of HO, which is believed to be the oxidizing species that attacks a meso-carbon in the heme, have suggested that this intermediate possesses a $(d_{xz},d_{yz})^4(d_{xy})^1$ electronic structure.[18] As has been pointed out above, Fe^{III} porphyrinates exhibiting an unpaired electron in the d_{xy} orbital place large unpaired electron density at the meso-positions.[60−62] Since this property of Fe^{III} porphyrinates helps to explain the attack suffered by the porphyrin meso-carbons by the coordinated peroxide in the Fe^{III}−OOH complex of HO, it is important that future efforts aimed at explaining the regioselectivity of the reaction also address the nature of the electronic structure of the highly reactive Fe^{III}−OOH intermediate.

Acknowledgment. This work was supported by NIH grants GM-50503 (M.R.) and AI 48551 (A.W.) and OCAST grant HR00-043 (M.R.). Funds for the Oklahoma Statewide Shared NMR facility were provided by the National Science Foundation (Grant BIR-952269), the Oklahoma State Regents for Higher Education, the W. M. Keck Foundation and Conoco, Inc.

Supporting Information Available: Figure S1, structures of the different biliverdin isomers; Figure S2, HMQC spectrum of *cd*-HO−CN reconstituted with heme derived from [1,2-^{13}C]ALA; Figure S3, HMQC spectrum of *cd*-HO−CN reconstituted with heme derived from [5-^{13}C]-ALA; Figure S4, WEFT−NOESY spectrum of *cd*-HO−CN. This material is available free of charge via the Internet at http://pubs.acs.org.

JA0274960

(60) Safo, M. K.; Walker, F. A.; Raitsimring, A. M.; Walters, W. P.; Dolata, D. P.; Debrunner, P., G.; Scheidt, W. R. *J. Am. Chem. Soc.* **1994**, *116*, 7760−7770.
(61) Walker, F. A. *Coord. Chem. Rev.* **1999**, *185−186*, 471−534.
(62) Walker, F. A. In *The Porphyrin Handbook*; Kadish, K. M., Smith, K. M., Guilard, R., Eds.; Academic Press: New York, 2000; Vol. 5, pp 81−183.